Received: 28 October 2024 | Revised: 2 December 2024 | Accepted: 8 January 2025 | Published online: 14 February 2025

RESEARCH ARTICLE

Archives of Advanced Engineering Science
2026, Vol. 4(1) 51–64
DOI: 10.47852/bonviewAAES52024621

BON VIEW PUBLISHING

Investigations of the Hybrid Effects of the Operational Parameters in the Radial Forging Process Based on the Validation of the Hardness Test

Saeed Darki[1,*] and Evgeniy Yurevich Raskatov[1]

[1]*New Material and Technology Institute, Ural Federal University, Russia*

Abstract: In this study, considering all the parameters in radial forging and a three-dimensional model has been simulated using the finite element method. By implementing an elastoplastic state for the specimen tube, parameters such as friction type, residual stress distribution, effective strain distribution, material flow velocity, its effect on the neutral plate, and the distribution of force in the die have been studied and analyzed. The effects of angle on the quality and characteristics of the specimen and the longevity of the die have also been obtained. Experimental results have been used to confirm the accuracy of the simulation. The results of the hardness test after forging were compared with the simulation results. Good agreement between the results indicates the accuracy of the simulation in terms of hardness. Therefore, this validation allows confirming the other obtained results for the analysis and prediction of various components in the forging process. After the validation and confirmation of the results through the hardness test, the hardness distribution was obtained by considering temperature changes and the effective strain on the specimen.

Keywords: finite element method, radial forging tube, residual stress, hardness microstructure

1. Introduction

Radial forging process (RFP) is a type of open die forging, and the product is surrounded by four dies. Thus, this machine is designed for round products such as tubes, shafts, stepped shafts, axes, gun bars, and rifle barrels. Reducing the diameter of specimens is the main purpose for using radial forging. Accordingly, the specimen is surrounded by four dies with special feed rates and rotational angles. Thus, when feeding stops, these dies reduce the diameter and deform the specimen via frequent strokes. Based on deformations, there are variations in specimen dimensions in both the radial and axial directions. In other words, geometry changes occur in both directions: in the radial direction, which changes the radius, and in the longitudinal direction, which changes the hollow shaft length.

Afrasiab et al. [1] found to create an axisymmetric model for the radial forging process of rods and an analytical method based on asymptotic analysis is suggested. This model accepts that the neutral plane's profile is not a planar cross-section of the workpiece and may forecast the radial deformation inhomogeneity. In order to assess the viability of the radial forging process, a link between the die angle, friction coefficient, and back-push stress has been established for the first time. Additionally, a novel technique has been put out that may locate the neutral plane much more quickly and easily than the conventional way. Du et al. [2] used numerical simulation to investigate how process factors (radial reduction Δh, rotation angle β, and friction coefficient μ) affect the forging process. The combination of $\Delta h = 0.25$ mm, $\beta = 21.68°$, and $\mu = 0.05$ is the optimum method. 0.241367 and 577.029 are the equivalent E and F, respectively. The forging load was decreased by 1.76%, and the total strain standard deviation was decreased by 14.25% as compared to the original procedure. Ghaei et al. [3] and Groche et al. [4] claimed to determine an upper bound limit for the deformation load in the situation of radial forging of rods and tubes, a novel model based on calculating the deformation work was created in the study. The goal of the applied conjoint forming technique is to include a functional element into a tubular section while concurrently shaping it to its final shape. As a result, good sensor linearity is guaranteed and lift-off of the sensor element in the event of tensile pressures during application is forbidden. According to Herrmann et al. [5], rotary swaging is a cold bulk deformation method where tools oscillate to reduce workpiece diameter. Lubricants are used for cooling, lubricating, and cleaning, but they have drawbacks like recycling and cleaning costs. Alternatives like structuring and covering instruments can replace lubricant functions. Jiang et al. [6] took advantage of the radial forging process in order to achieve a new recrystallization and partial melting technique that was used to create axial 2A50 aluminum alloy semi-solid billets. The microstructure properties of the forged and isothermal-treated materials were examined. The results showed that heating the sample to 585 °C for 10 min replaced original elongated grains with spherical equiaxed grains

***Corresponding author:** Saeed Darki, New Material and Technology Institute, Ural Federal University, Russia. Email: darki@urfu.ru

and high angle grain boundaries. The grains' coarsening rate constant was 378.5 $\mu m^3/s$. Kumar et al. [7] presented the behavior of magnesium alloys with properties of lighter weight and higher specific strength in the manufacturing processes, especially within the radial forging machine. This overview focuses on the mechanical characteristics and microstructure development of magnesium alloys through various forging processes, including open die forging, closed die forging, multi-directional forging, isothermal forging, and radial forging, resulting in improved forgeability. Li et al. [8], Liu et al. [9] and Li et al. [10] investigated on hollow stepped gear shafts for automobiles focusing on lightweight construction. The orthogonal design technique was used to choose the best combination of parameters, including radial reduction, rotation rate, and starting temperature. The study found that the outermost and innermost zones of cross-sections had the highest and lowest effective strains, respectively. A starting temperature of 780 °C, a rotating rate of 21°/stroke, and a radial reduction of 3 mm are found to be the ideal forging parameters. Accordingly, Mahdavi and Haghighat [11] illustrated that the drawing force is decreased by increasing the die angle; after an increase of almost 6°–8°, the drawing force will increase through the drawing bar. The maximum reduction on the bar and strain hardening are directly proportional, while most scientists have studied through the 2D mathematical model that cannot cover all variations during the process. In this regard, Moumi et al. [12] studied the material flow of the swaging process via FEM. The neutral plate was subjected to a variety of friction and feed velocities. Moreover, this simulation, which was based on a 2D dimension cloud, describes various process parameters. By increasing the velocity of feeding, the rate of neutral plate location change decreases. One of the essential boundary conditions in order to the simulation of RFP is the assumed flow material within the process. Thus, Sanjari et al. [13] claimed through a microstructural investigation, by increasing the friction coefficient, the homogeneity of deformation will increase. Moreover, they showed that increasing the friction factor can increase the effective strain plus the variations of strain range will also increase. On the other hand, to obtain minimum inhomogeneity and radial force, they used FEM results for optimization via Taguchi neural networks and validated by experimental hardness tests. They thus showed that high friction on the inner side is the cause of high inhomogeneity. The die angle makes the most contributions to the optimized parameters. On the other side, Wang et al. [14] used the FORGE software to simulate the penetration performance of radial forging for 6063 wrought aluminum bars. The study examines the effects of variables like billet temperature and forging ratio on hammer load and effective stress. Results show that effective strain at the center and edge of the RF-deformed billet increases, but the strain at the edge decreases with increasing speed. The study recommends low billet temperature and high forging ratio for optimal performance. The RF-deformed blank shows a 91.19% penetration performance improvement ratio. Also, the calculation of the field velocity of material continuously through the upper band method can provide more accurate predictions than the parallel velocity field while showing the material's streamline. Wu and Dong [15] and Wu et al. [16] illustrated the location and movement of the neutral plane with different diameter reductions via the upper bond method. Also, the convex value at the end of the model increases if the reduction rate and feed rate increase, and also, the material flow more than the feed rate depends on the reduction rate. While the FEM have fewer errors than the upper bound method based on validation by experimental outcomes, Yang et al. [17–19] analyzed radial forging with rectangular die and specimens through the upper bound method and FEM. They showed that by increasing the die angle, the axial flow of the material will decrease. They showed that the length of overlapping can increase the connecting strength; however, if the necking for aluminium increases by more than 45%, the aluminium will fail. Zou et al. [20, 21] analyzed the microstructural characterization of ZK60 Mg alloys under radial forging (RF) using a regionalized strain field model. The study involved treating ZK60 magnesium alloy bars under various stresses using RF at 300 °C. The results showed that dynamic recrystallization dominated the subsequent deformation process, while twinning dominated the early phases. The grains in different radial sections gradually refined, eventually developing into a bimodal-grained structure with coarse and fine grains. The c-axis of the deformed grains rotated in the radial direction, and the texture of the RFed bars changed as the RF strain rose. After the three passes, better mechanical qualities were also attained, such as increased tensile strength (341 MPa) and ductility (27.1%) values. Zuev et al. [22] explored the use of radial forging in producing Ti alloy rods without mechanical treatment. It analyzes the plasticized metal flow and microstructural development in various rod sections using hot pressing and RF. Metallography and X-ray diffraction reveal the alloy's two-phase condition, revealing radial forging's ability to change the alloy's phase composition. The study concludes that radial forging is a reliable technique for achieving high-quality rod surface and homogeneous fine-grained structure.

Although in the previous investigation, the FEM and parameters impact have been considered, they have neglected the interaction of the parameters with each other or the implementation of the most accurate model and method. Therefore, it is necessary to examine this complex process through variations in the essential parameters that influence the process and to take a comprehensive view of the effects of these changes on the specimen. Therefore, a 3D visco-elastoplastic model was chosen, as it predicts and characterizes this process and all factors affecting it with high accuracy. In addition, the results were validated through the two parameters of total load and microhardness. The experimental and simulation results are in agreement, indicating the accuracy of the simulation and prediction process. Thus, as the principle targets of this article, the mathematical model has been established to the analysis of the radial forging parameters, and on the other side, the variations of die angle and types of friction have been simulated to obtain optimize angle according to the requested demands.

2. Parameters and Methodology of Radial Forging Process

RFP is one of the basic tools for metal deformation. This machine includes four dies, which surround the specimen and make consecutive strokes on it in order to increase material strength. There are many types of radial machines with different work functions, such as hot or cold forging, hydraulic or mechanical stroking and rotary swaging. The radial forging equipment implemented in the simulation is shown in Figure 1. The mandrel is fixed to the specimens and then four dies deform the product with consecutive strokes.

The quality and dimension precision depend heavily on the process parameters. These parameters directly affect the longevity of the die and forging machine by helping to calculate the residual stress and principal stress on the other components. As such, investigating die geometry through 3D finite element simulation, which can present all interactions between the equipment during operation, is essential. This numerical simulation has been implemented in the software DEFORM-3D V11.0. Moreover, regardless of the geometric characteristics of the workpiece, other end-product features, such as residual stress and microstructure, can

Figure 1
(a) Components and motion direction of elements of the radial forging process. (b) The 3D section of the simulation with the mesh grid of the workpiece during the simulation process

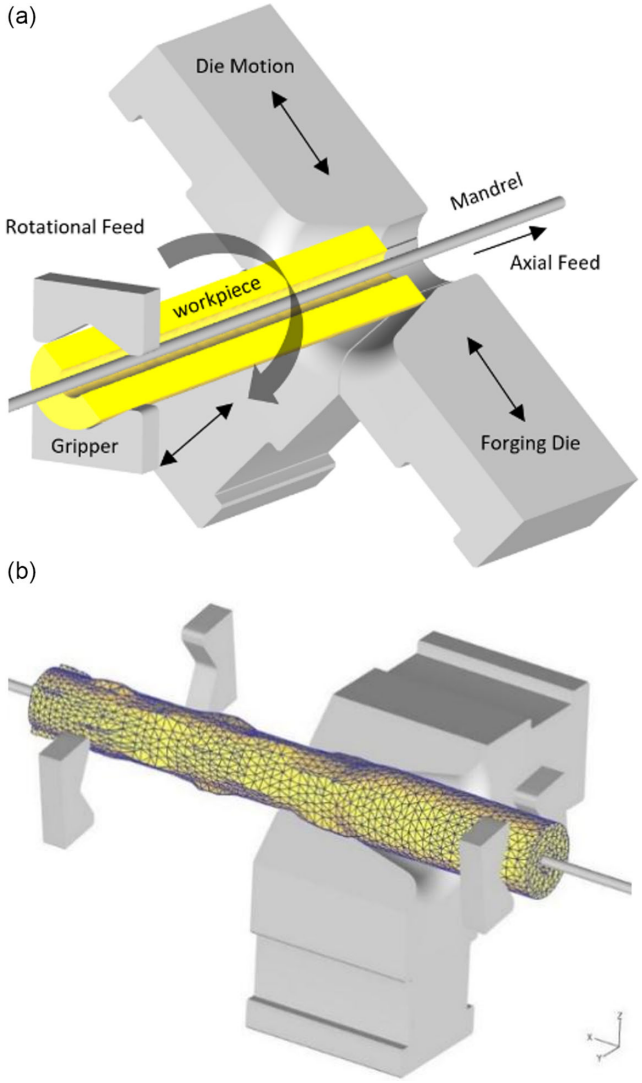

be affected by the design criteria of the radial forging machine. The geometry parameters of the die are presented in Figure 2.

In this figure, the three sections of the die are shown. These have three duties: sinking, forging, and sizing. The die angle has direct effects on sinking and forging. It can also change the coordinates of the neutral plane according to the material flow. The section of the die has a direct relationship with the feed rate and homogeneity deformation of the specimen's surface. The important factors in RFP such as total force, die angle, type of friction, and value of the coefficient friction can have a principal role in microstructure hardness, material flow, residual stress, and the amount of increased strength of the specimen. Therefore, these factors are discussed below via a comparison between different types of friction and the value of parameters.

Two types of friction are considered: coulomb (sliding) and constant shear (sticking). The coulomb law describes the contact forces between two objects under elastic deformation. However, these objects can be elastic-plastic: one is elastic and the other is rigid during elastic deformation. Moreover, the simulation of sheet forming has been recommended for this type. The frictional stress is calculated to describe the contact of two plastic or porous objects by the flow stress of the object. The frictional force in the coulomb law model is defined by:

$$f_s = \mu P \tag{1}$$

where f_s is frictional stress, P is the interface pressure between two bodies, and μ is the friction factor.

Constant shear friction includes highly precise measurement and modeling of bulk-forming simulations. The frictional force in the constant shear law is defined as follows:

$$\tau = m\sigma_y/\sqrt{3} \tag{2}$$

where m is the frictional coefficient and σ_y is the normal yield stress of the material. This states that friction is a function of the yield stress of the deforming body.

The material used in the simulation was DIN-16CrMo4 steel. The material parameters are shown in Table 1.

The initial forging temperature was 900 °C. In the current study, the flow stress was obtained through the Johnson-Cook equation:

$$\overline{\sigma} = (A + B\overline{\varepsilon}^{n})\left(1 + C\ln\left(\frac{\dot{\overline{\varepsilon}}}{\dot{\varepsilon}_0}\right)\right)\left(\frac{\dot{\overline{\varepsilon}}}{\dot{\varepsilon}_0}\right)^{\alpha}(D - ET^{*m}) \tag{3}$$

where $T^* = \left(\frac{T-T_{room}}{T_{melt}-T_{room}}\right)$ and $(\overline{\sigma})$ is the flow stress of DIN-16CrMo4 steel. Effective plastic strain rate $(\dot{\overline{\varepsilon}})$ and (T_{melt}) is melting temperature and $A,\ B,\ C, D, E, n, \alpha, \dot{\varepsilon}_0$ are model coefficients of material and $T,\ m$ are thermal softening of the material. Thus, the flow stress chart has been presented in Figure 3.

Figure 2
Die angle and three typical zones in the radial forging process with the axial cross-section of the workpiece, die, and mandrel

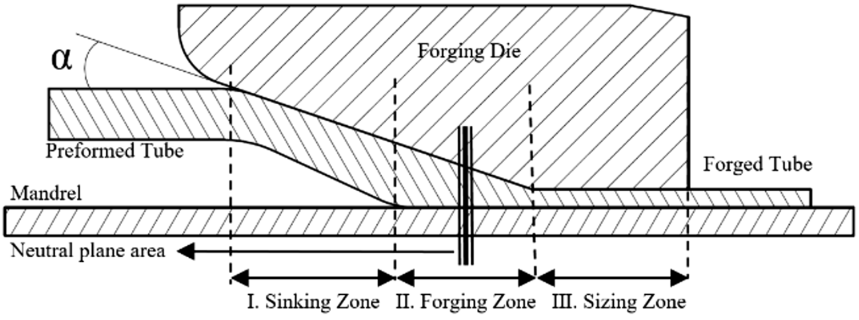

Table 1
Mechanical properties of the used material

Density (kg/m^3)	7870
Young's modulus (GPa)	212
Poisson's ratio	0.3
Specific heat (J/kg/· C)	750
Conductivity (W/m/· C)	15
Melting temperature (C)	1450–1510
Inelastic heat fraction	0.9
Thermal expansion coefficient (1/· C)	11×10^{-5}
Yield Strength (Mpa)	275

As mentioned, parameters such as residual stress can have a direct impact on the strength of the specimen and its longevity. Residual stress is a function of multiple factors such as temperature, die angle, total force, and friction, and the effect of these factors has presented and analyzed separately. Thus, material flow velocity, one of the factors used for calculating the microstructure of the material and the amount of hardness, is examined in the following sections. Moreover, the effect of die angle on the neutral plane coordinates via material velocity and the location of the neutral plane relative to the die zone is presented. In terms of the friction, the effects of different values of coefficient friction on temperature, residual stress, and specimen quality are shown. The most accurate and most suitable types of friction have been determined by comparing the simulation results for two types of friction and their effect on forging force. It is worth mentioning that the type of friction has been determined via using the simulation results closest to the actual results. In this investigation, the simulation has been validated by comparing the experimental hardness values and the simulated hardness values. Specimen hardness itself is a function of different parameters; however, it is expressed here using temperature and effective strain. For this purpose, a hardness test was designed to measure hardness at several points along the specimen. In the previous investigations, the effective strain values were measured at several points along with the specimen. Therefore, the hardness was calculated via the hardness function and measured values. Finally, as simulation verification, the experimental and measured graphs were compared. Other outcomes of the simulation could be cited, such as residual stress and the analysis of other influences on specimen quality.

In general, due to the complex nature of the process, which is a function of overlapping multiple factors, there is no explicit concept

Figure 3
Flow stress-strain curve of DIN-16CrMo4 steel at 900 °C. With the different strain rate based on the Johnson-Cook equation

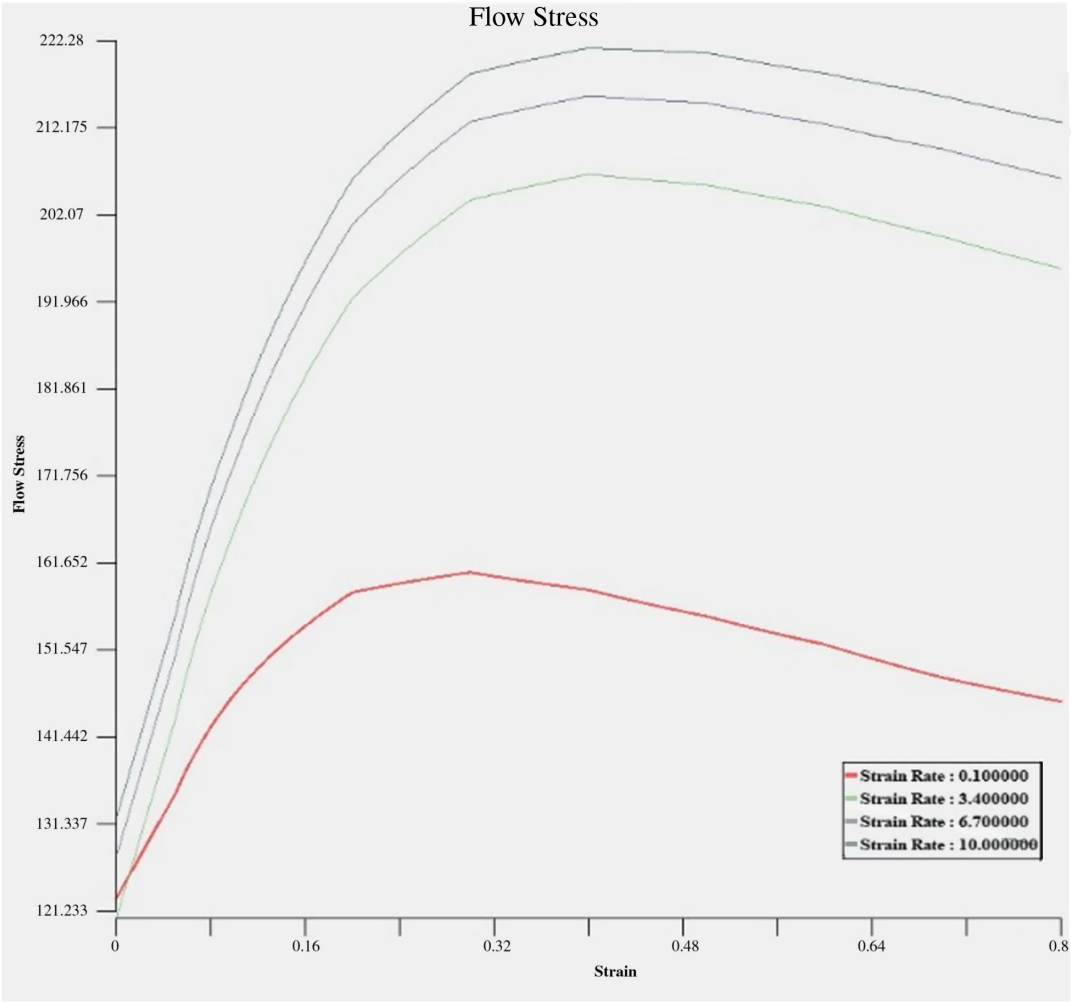

of optimization for the whole process. When expressing an optimal value for die angle, total force, or feed rate, other parameters may be neglected.

Thus, it seems that the best way to study this process is a comprehensive analysis of the effects of the parameters on each other. Due to the wide potential application of this process, it is worthwhile attempting to increase the quality of the specimen and meet working conditions.

3. Numerical Analysis and Experimental Method

There are several methods for analyzing the forging process, such as the upper bounds methods, the slab method, and others investigated and implemented by previous authors, but the most accurate results are obtained by FEM. This method provides a comprehensive view of all the phenomena and conditions during forging.

By applying appropriate boundary conditions and simulation parameters, simulation accuracy can be significantly increased. Therefore, conditions such as friction in all process components (the back spring pressure of manipulators and mandrel and their impacts on material flow) are considered. Using specimen temperature, the heat transfer between the mandrel and the specimen has been calculated while this can have a direct effect on specimen hardness. Therefore, the viscoplastic model has been used for a more accurate examination of the material flow rate. Therefore, the Von Mises yield criterion has been implemented in order to flow rules. The relation between the essential matrices of FEM has been presented by Darki and Raskatov [23, 24].

Although other models such as rigid plastic or elastoplastic ones have been used in most previous studies, these do not have the necessary precision to determine neutral plate coordinates. In other words, it can be stated: (i) the material has viscoplastic behavior during the process; (ii) there is heat transfer during the forging process; and (iii) the dies and mandrel are assumed to be made from a rigid material. For the calculations and observations, RS has been defined as the final stresses on the product and residual stresses during the process. In most RFP simulations, the effects of die cooling are ignored due to the relatively short contact time between the die and the product.

In order to investigate the effects of the die angle, six different specimens are considered: these are described in the following table. Also in this simulation, two manipulators are considered. Each manipulator has a spring in order to control the movements and feeding of the workpiece in two directions: axial and rotational. In order to reduce the error of the simulation results and also bring the operating conditions closer to the industrial and real process, and according to the previous investigation and the introduction, the material phase is modeled as viscoplastic of the workpiece as the main boundary condition. The other geometrical and dynamic boundary conditions are principally recommended by other previous investigations and experimental results. However, the range of boundary conditions was determined by other references, but the optimization conditions were unknown and defined as targets of the current study. Other geometrical dimensions of the components are listed in Table 2. It should be noted that all measurements in the simulation after each stroke on the specimen have been taken to show that stroke effect remains the same over the length of the tube. The length of the specimen is 200 mm. Also, the simulation dynamic parameters such as rate of stroking (stroke per min), rotating feeds, axial feed (mm), number of strokes, number of passes, rotation per pass are respectively: 400, 36°, 20, 12, 2, 10°.

To validate the simulation, the hardness criterion is measurable. For this purpose, two auxiliary criteria, effective strain and temperature, have been used. These two criteria have an impact

Table 2
Geometry parameters of the mandrel, specimen, and die

Outer diameter (mm) – Reduction rate	30 – 20%
Inner diameter (mm) – Reduction rate	10 – 60%
Outer diameter for mandrel (mm)	4
Length of die (mm)	70
Length of die land (mm)	25
Die angle	5°, 10°, 12.5°, 15°, 20°, 90°

on the hardness of the specimen. For this reason, a tube with the geometry of the simulated specimen was used. The length, radius, and thickness of the sample were measured by a hardness tester. The following is a view of the measured sample in Figure 4.

Figure 4
A sample of a forged tube of two different cross-sections for comparison before and after the radial forging process. The tube shows the sections required for hardness testing

The experiment used standard temperature conditions and a portable hardness tester to measure the hardness in different sections at random points in Figure 5. According to the dimensions of the tube, the impact device type D has been considered to measure the hardness of the tube in different section through the variations of effective strain. The components of a type D impactor are shown in Figure 6. For this purpose, about 50 points were marked and measured. It should be noted that the die angle for this

Figure 5
Hardness tester with impact device type D and connecting cable

Figure 6
(1) Trigger button (2) Loading shell (3) Guide tube (4) Spool (5) Connecting cable (6) Striking body (7) Support ring

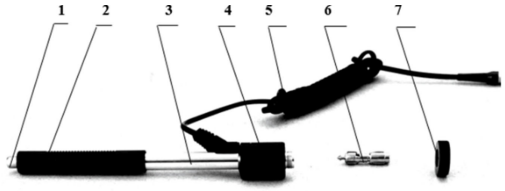

test was 5°. After measuring the radius variations and calculating the effective strain on the sample, the hardness-strain curve was obtained. The effective strain equation is given below [23]:

$$\bar{\varepsilon} = \frac{\sqrt{2}}{3}\sqrt{(\varepsilon_1 - \varepsilon_2)^2 + (\varepsilon_2 - \varepsilon_3)^2 + (\varepsilon_3 - \varepsilon_1)^2} \quad (4)$$

where $\varepsilon_{1,2,3}$ are the principal strains and $\bar{\varepsilon}$. is the effective strain. By measuring the different strains on the specimen through simulation and placing them into the hardness function, the hardness value of the specimen is shown. To apply the temperature effects to other types of die and to show the distribution of hardness in all sections of the specimen, the hardness-temperature curve was defined by the hardness values obtained for different strains and temperature values. The hardness distribution is thus rendered visible by the temperature and strain effects. After comparing the experimental and simulation results and verifying the accuracy of the simulation, the same method of the simulation was used to analyze the other parameters. In the previous investigation expressed the following equation as the hardness function, where (Hv) is hardness and $(\bar{\varepsilon})$ is effective strain.

$$Hv = -60.7\bar{\varepsilon}^2 + 119.1\bar{\varepsilon} + 115.1 \quad (5)$$

Table 3
Specimen geometry and contact force via the experimental and simulation results of process

Sample type	Outer radius of perform (mm)	Inner radius of perform (mm)	Out radius of product (mm)	Inner radius of product (mm)	Die force (KN)
Experiment	18	14.6	13.70	9.30	385.00
FEM	18	14.5	13.66	9.45	366.480

4. Results and Discussion

In regard to the comparison between the error percentage of the simulation and experimental results; the current simulation procedure can be used for deloping and expanding the investigation of parameters such as coefficient friction and die geometry. This simulation has been verified by comparing it with experimental results for cold RFP, which is presented in Table 3 [1, 23].

Table 3 has illustrated the dimensions of experimental and mathematical model for a cold forging sample. According to the obtained results, there is a good correspondence between the experimental and simulation results in the peak contact force through FEM simulations. Figure 7 displays a radial forging machine to obtain the experimental contact force. From the obtained results, the difference is less than 5%, which might be due to a thermal effect.

Since the contact force is one of the principal criteria of RFP in order to analyze of process, the examination of contact force vs radius reduction leads to an estimate of the quality of forged tube and dimensions of the radial machine. Therefore, Figure 8 displays the contact force of experimental results and FEM results vs reduction outer radius of tube, and on the other hand, the function of this issue has been obtained to estimate applied force vs reduction radius for the used material. According to this comparison, the current simulation results have less error rather than other methods and previous investigation.

4.1. Friction impacts

It is necessary to determine the most appropriate type of friction for the simulation before examining the effect of friction on temperature, forge force and material flow velocity. Hence, two types of friction (coulomb and shear) were simulated. In this case, the simulated forging force was measured and the most

Figure 7
Radial forging machine with a feeding system during the practical test

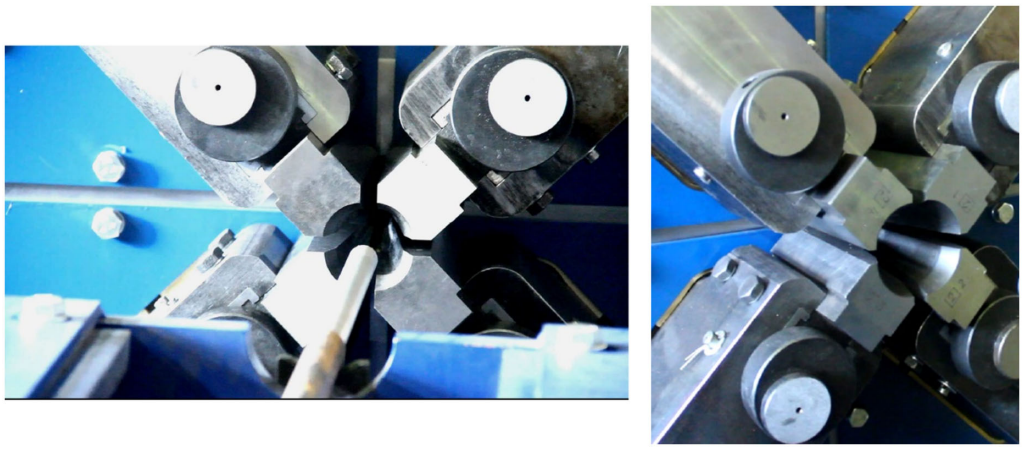

Figure 8
The reduction radius rate vs applied force with an estimate by a 3-degree polynomial function

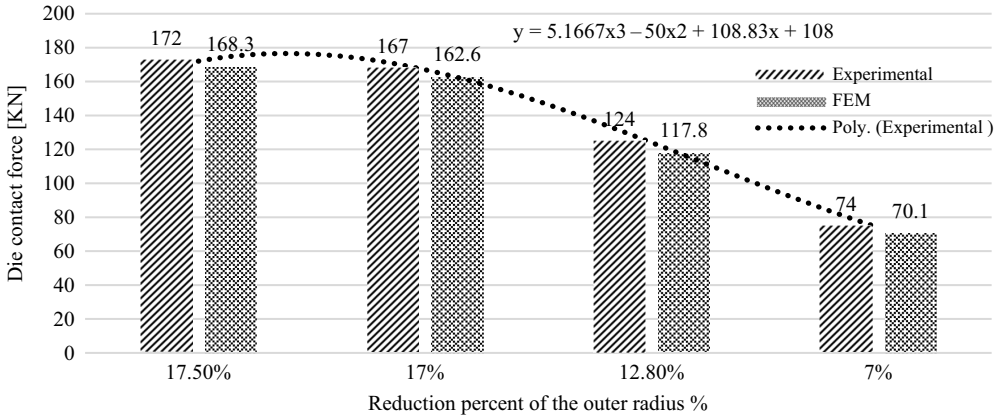

Figure 9
Total load vs. time for two types of friction. First pas; at boundary condition: T = 900 C, friction coefficient = 0.4, axial feed = 25 mm, rotary feed = 40 degrees per stroke, stroke/ pass = 8, forging speed = 150 mm/sec, DIN-16CrNi4

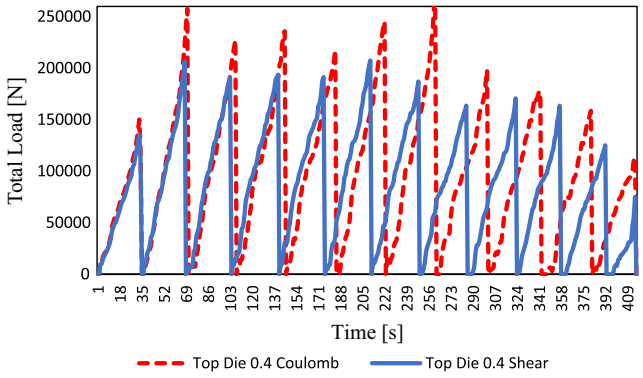

appropriate type of friction was determined by comparing it with the experimental value. Given the higher values of the forging force for coulomb friction and the inconsistency with experimental values, it can be concluded that this type of friction is incapable of describing this process. On the other hand, due to shear friction's low error percentage, it can be claimed that the shear friction has a higher accuracy for the simulation of RFP. Thus, this friction model will be used to analyze this process with the assumption of a 0.4 friction coefficient. The comparison of both types of friction is shown in Figure 9.

As shown in Figure 10, as the friction coefficient increases, the forging force increases sharply with each stroke. Thus, the friction coefficient has a direct relationship with the forging force. Moreover, the total time increases as the friction coefficient increases.

Material flow velocity is one case where friction can have a direct and significant impact. For this reason, three different friction coefficient values, 0.4, 0.6, and 0.8, were considered. It should be noted that a die angle of 15° was assumed and the velocity was measured in the axial direction after the neutral plane. All values belong to the first pass. As shown in Figure 11,

Figure 10
The variations of the total load vs. time for different values of shear friction. At boundary condition: T = 900 C, friction coefficient = 0.4, axial feed = 25 mm, rotary feed = 40 degrees per stroke, stroke/pass = 8, forging speed = 150 mm/sec, DIN-16CrNi4

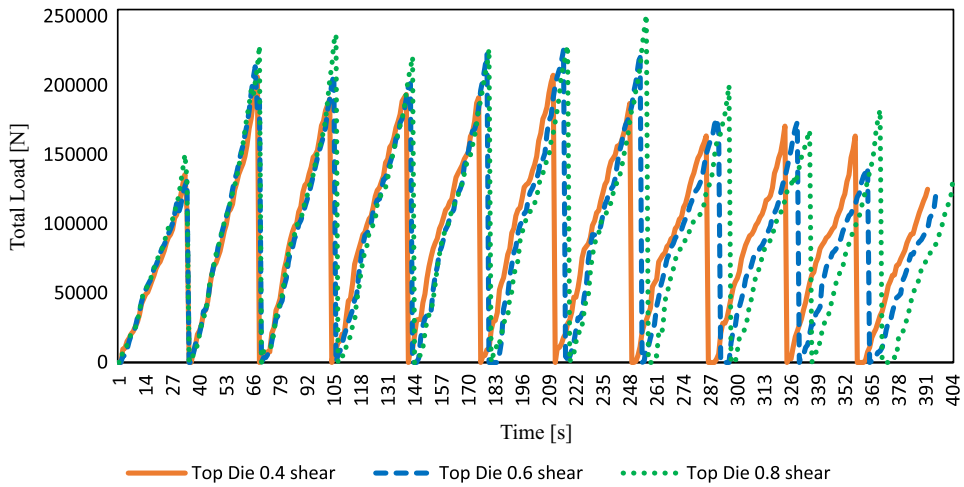

Figure 11
The axial material velocity vs. length of the workpiece for different shear frictions of 0.4, 0.6, 0.8, $\alpha = 15°$, in the sizing zone and during the first pass

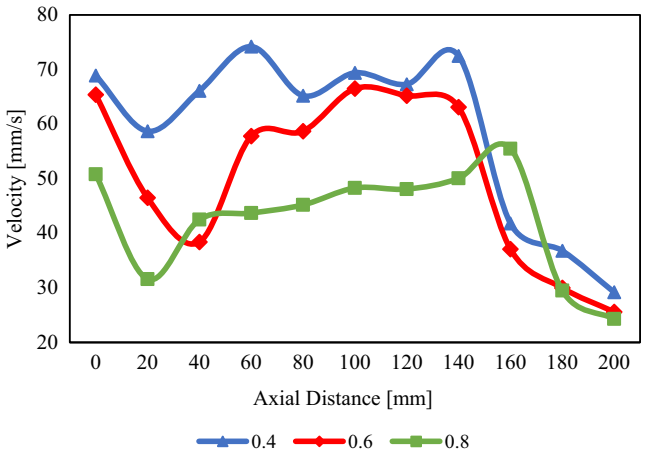

Figure 13
Distribution of residual principal stress vs. length of tube for different shear friction values 0.4-0.6-0.8 for die angle $\alpha = 15°$

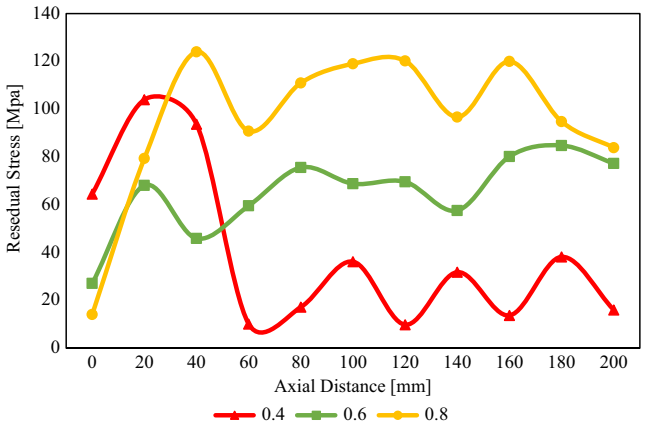

as the friction coefficient increases, the material flow velocity decreases. The highest axial flow velocity of the material is produced by the lowest friction value.

Figure 12 shows temperature variations based on different shear friction values. As expected, with increasing friction, the temperature increases, which in itself can be a confirmation of the correct simulation method. The temperature distribution is also considered on the outer surface of the specimen. Calculating the temperature distribution and the maximum temperature for different friction values is needed to estimate specimen hardness. This analysis will be a criterion for controlling specimen temperature with respect to maximum allowable temperature.

Figure 13 illustrates the residual stress variations based on different friction values. The highest residual stress distribution values are produced by the highest friction value while the lowest is for the 0.4 shear friction coefficient. However, the non-uniformity of this stress distribution throughout the specimen can be considered a factor in reducing specimen quality. The 0.6 coefficient has a uniform RS distribution, which leads to higher specimen stability under critical loads.

Figure 12
Distribution of maximum temperature on the outer surface of tube in axial direction vs. different shear friction values 0.4-0.6-0.8

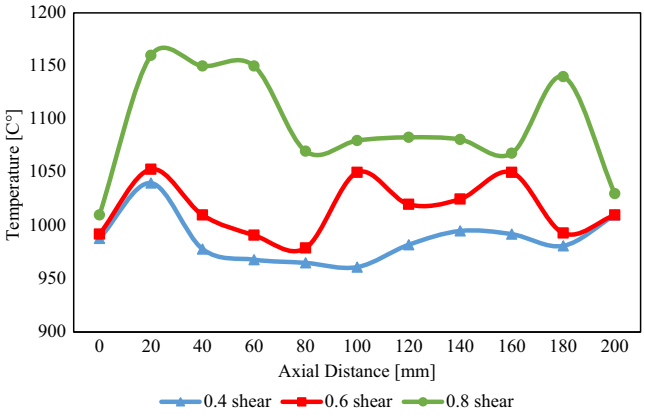

4.2. Die angle impacts

As mentioned, one of the purposes of this simulation is to investigate the effects of die geometry on the specimen. Figure 14 presents the effects of the (α) angle on density changes. Assuming that mass is constant throughout the process and the volume is reduced during operations, density will increase. The increase in density reflects the improvement of the specimen's microstructure. Figure 14 shows that an angle of 10° leads to the highest density. After 10°, the gradient of the density curve declines and the lowest value density is produced by an angle of 20°.

Figure 15 shows the forging load along the workpiece per stroke. The shear friction coefficient is 0.4. As the chart shows, the highest forging load is 5° and the lowest 20°. There are more oscillations at 20° than at 5°, which can produce additional vibrations in the forging machine. Therefore, it is necessary to study the oscillations of the applied force when considering the maximum amount of force required.

Due to the importance of the surface smoothness of the specimen and in order to avoid complicated operations, it is important to examine the dimension changes of the specimen and its deformation from a strain perspective. For this reason and given the inhomogeneity factor defined by Equation (6), the presentation of effective strain distribution should be a measure of surface quality after forging:

$$IF = \frac{\bar{\varepsilon} - \varepsilon_{min}}{\varepsilon_{min}} \tag{6}$$

$\bar{\varepsilon}$ is effective strains on the surfaces contacting the specimen and the die and ε_{min} is the minimum strain on the radial direction of the specimen.

In Figure 16, effective strain distribution along the specimen at different angles is displayed. The most uniform deformation belongs

Figure 14
Density vs. different die angles. At boundary condition: T = 900 C, friction coefficient = 0.4, axial feed = 25 mm, rotary feed = 40 degrees per stroke, stroke/pass = 8, forging speed = 150 mm/sec, DIN-16CrNi4

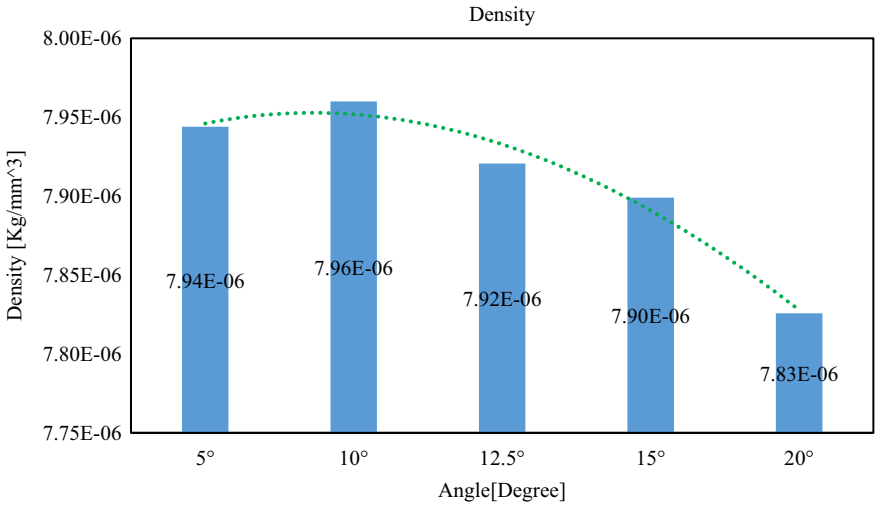

Figure 15
Total load along the specimen at different die angles. At boundary condition: T = 900 C, friction coefficient = 0.4, axial feed = 25 mm, rotary feed = 40 degrees per stroke, stroke/pass = 8, forging speed = 150 mm/sec, DIN-16CrNi4

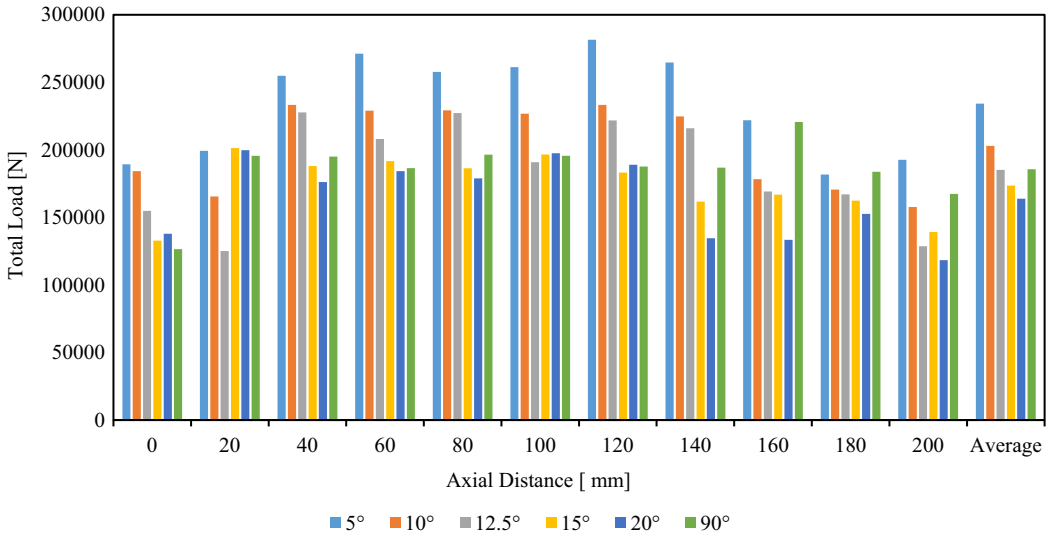

to the 15° angle. The 5° and 90° angles have the highest strain oscillations, indicating surface non-uniformity.

In Figure 17, the temperature distribution along the specimen is shown at different angles. As is clear, the lowest average temperature upon each stroke is at 15° and the highest at 90°. As the angle increases up to 10°, the temperature increases while for the angles over than 10° the temperature decreases. It is worth mentioning the die with the 90° doesn't follow these variations due to a lack of all section of geometry. 15° leads to the lowest temperature distribution. The temperature distribution increases for angles above 15°.

Material flow velocity can express the position of the neutral plate and the form of the microstructure particles. The coordinates of the neutral plate can change the stress distribution on the die and thus can be used to estimate die longevity. The flow velocity has a direct influence on the quality and shape of microstructures. Due to the pattern of material velocity distribution, as the die angle increases up to 15°, the material flow velocity decreases while for over than 15° the range of velocity increases. Figure 18 illustrates this trend.

Yang et al. [18] claimed that at an angle of 5°, the neutral plate is in the forging section. According to the obtained results, as the angle increases, the position of the neutral plate moves from the size section to the forging section. Similarly, as the angle decreases, the distance of the neutral plate from the edge of the pipe increases. On the other hand, as the die angle increases, the angle of the distribution of velocity zones in the material increases (β), which in turn can affect the shape of the granular

Figure 16
Distribution of effective strain along the specimen at different die angles. At boundary condition: T = 900 C, friction coefficient = 0.4, axial feed = 25 mm, rotary feed = 40 degrees per stroke, stroke/pass = 8, forging speed = 150 mm/sec, DIN-16CrNi4

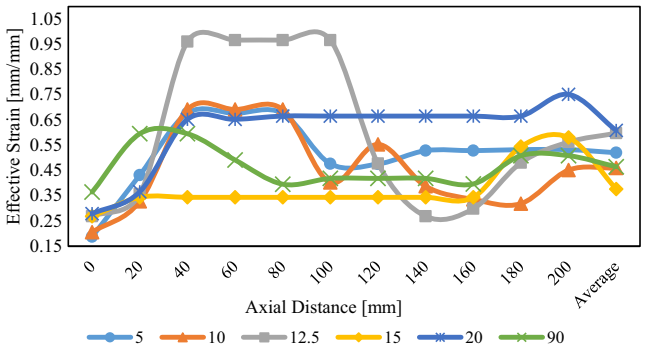

Figure 17
Distribution of temperature along the specimen at different die angles. At boundary condition: T = 900 C, friction coefficient = 0.4, axial feed = 25 mm, rotary feed = 40 degrees per stroke, stroke/pass = 8, forging speed = 150 mm/sec, DIN-16CrNi4

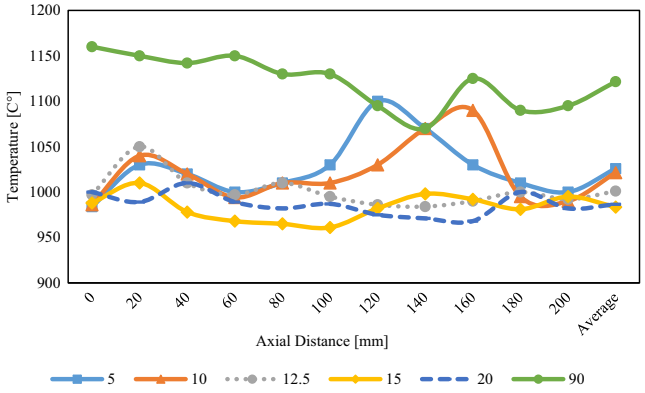

Figure 18
Distribution of velocity along the specimen at different die angles. At boundary condition: T = 900 C, friction coefficient = 0.4, axial feed = 25 mm, rotary feed = 40 degrees per stroke, stroke/pass = 8, forging speed = 150 mm/sec, DIN-16CrNi4

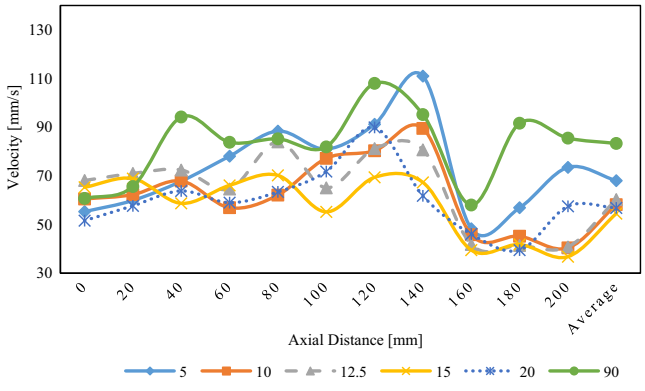

material, thereby establishing a criterion for describing the microstructure. Figure 19 illustrates this phenomenon, the variation of the angles of the material flow layers, and the position of the neutral plate.

Residual stress is one of the parameters which can determine the longevity of the specimen after forging. Hence, residual stress distribution was measured after each stroke. Based on examining the effect of die angle on residual stress, Figure 20 shows the lowest value of residual stress was produced by an angle of 15°. Thus, by increasing the angle to 15°, residual stress decreases and then increases again for angles above 15°. It can also be claimed that an angle of 15° leads to the most uniform stress distribution. This can be a strong indicator of quality.

Just as angle changes have different effects on the specimen, these changes can also occur in the forging machine. Residual stress is an important parameter in die analysis. For this purpose, the maximum stroke amplitude for different angles in the first pass was considered and the residual stress in the same motion range was calculated. These variations are displayed in Figure 21. According to the results, the lowest value is produced by an angle of 12.5°. After this angle, the residual stress on the die increases significantly while there are no drastic changes for angles lower than 12.5°.

4.3. Hardness

Tube hardness analysis consists of two parts: analysis of the experimental results and analysis of the simulation results. In the experimental section, after calculating the effective strain value and measuring the hardness of the specimen with a hardness tester, the curves of the effective strain and hardness were obtained. Figure 22 expresses the strain-hardness curve obtained via 4 approximated polynomials. Similarly, Figure 23 shows the measured values by hardness tester between 0.2 and 0.3 [mm/mm] effective strain. Finally, the investigation and analyses have been validated by comparing the hardness-strain curve obtained through the simulation and the experiment. Given the strong agreement between the simulation and experimental results, it can be claimed that other simulation results are reliable for analyzing radial forging in industrial conditions.

Figure 24 shows the hardness distribution on the specimen's surface along the longitudinal line. According to the results, the lowest value for hardness distribution on the surface is related to an angle of 15°. On the other hand, this angle leads to the highest hardness uniformity. The uniformity of the hardness distribution can be a criterion of microstructure quality and the uniformity of granularity in the surface layers.

5. Conclusion

In this research, a three-dimensional model of a radial forge was simulated and subjected to numerical analysis based on FEM. The simulation and experimental results were compared to each other and the strong agreement of the obtained results indicates the accuracy of the simulation for analyzing and predicting the characteristics of specimens based on the required conditions. In this research, an attempt has been made to analyze all the parameters affecting this process in order to provide the specimen with the required characteristics. These results can improve the application of a radial forging machine and optimize the parameters

Figure 19
(a), (b), and (c) 5, 15, and 20 die angles, respectively, vs. the distribution of velocity and the distance between the end of the specimen, the neutral plane, and the angle of velocity

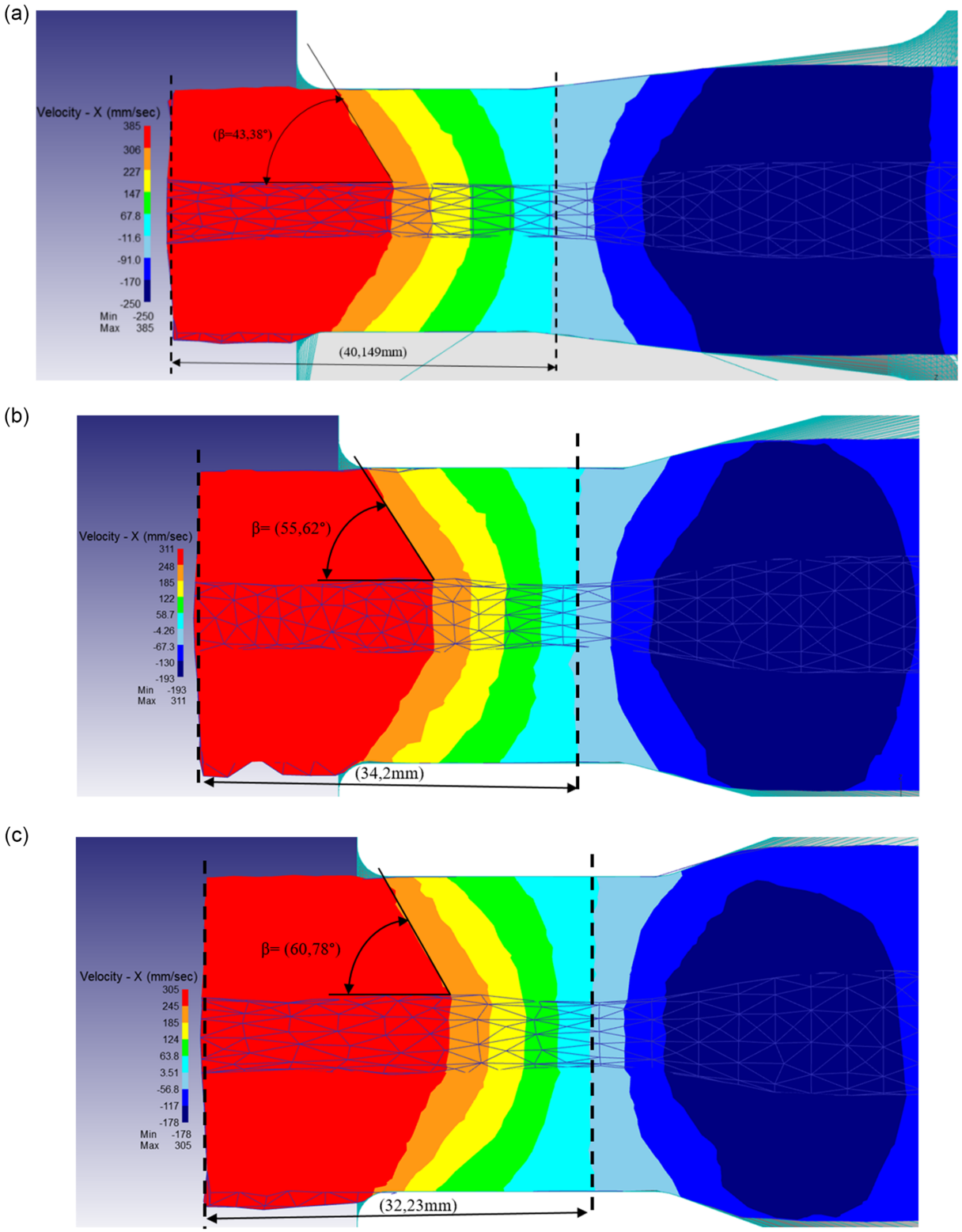

Figure 20

Distribution of residual stress along the specimen at different die angles. At boundary condition: T = 900 C, friction coefficient = 0.4, axial feed = 25 mm, rotary feed = 40 degrees per stroke, stroke/pass = 8, forging speed = 150 mm/sec, DIN-16CrNi4

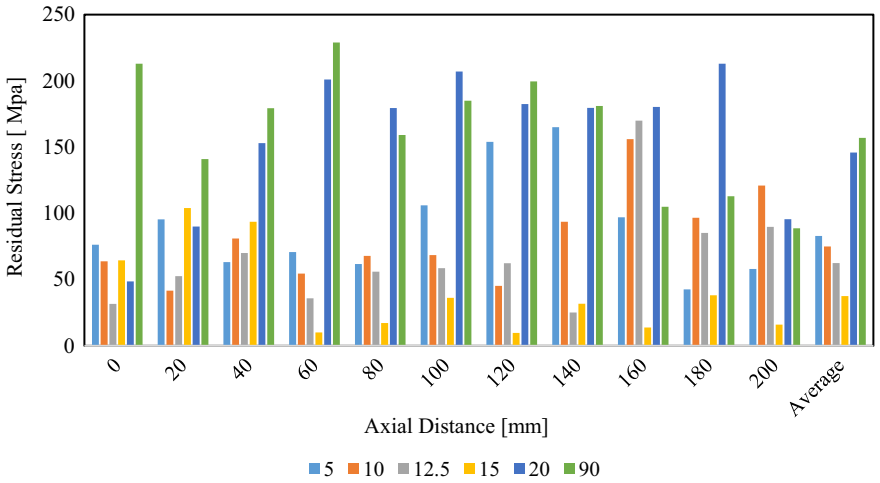

Figure 21

Die distribution of residual stress for maximum stroke at different die angles. At boundary condition: T = 900 C, friction coefficient = 0.4, axial feed = 25 mm, rotary feed = 40 degrees per stroke, stroke/pass = 8, forging speed = 150 mm/sec, DIN-16CrNi4

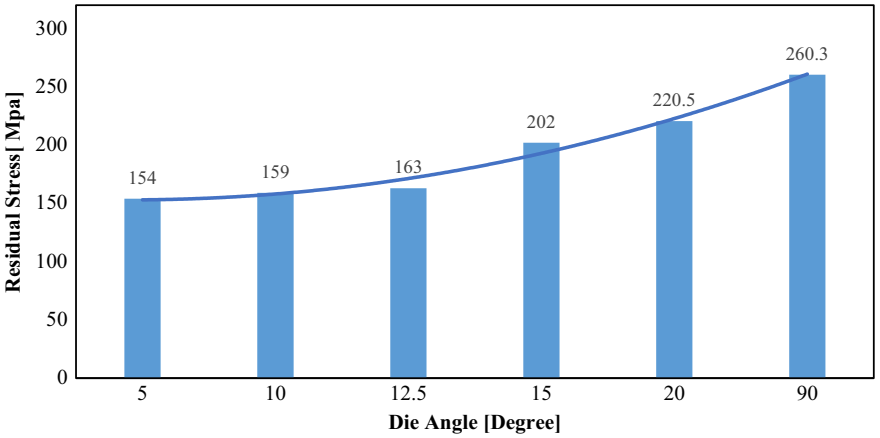

Figure 22

Comparison of hardness-strain experimental curve (measurement) and simulation values by an approximate fourth-order polynomial. At boundary condition: T = 900 C, friction coefficient = 0.4, axial feed = 25 mm, rotary feed = 40 degrees per stroke, stroke/pass = 8, forging speed = 150 mm/sec, DIN-16CrNi4

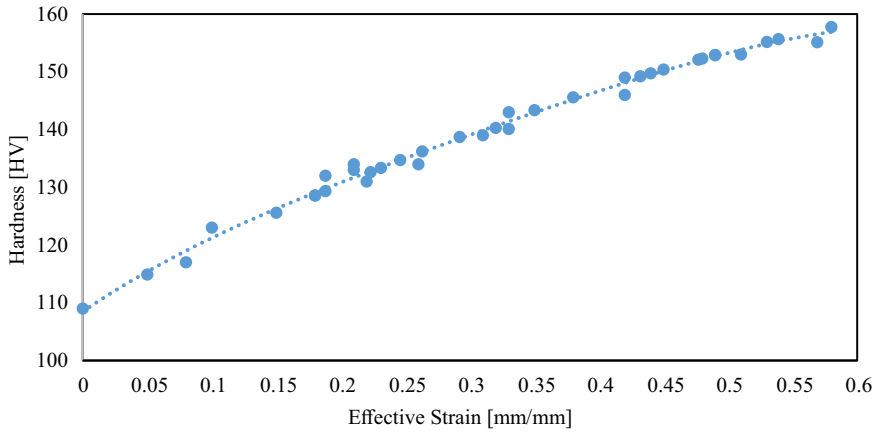

Figure 23
The displaying of measured hardness value s[HV] by tester in computer by impactor type D. For 0.2–0.3 [mm/mm] effective strain

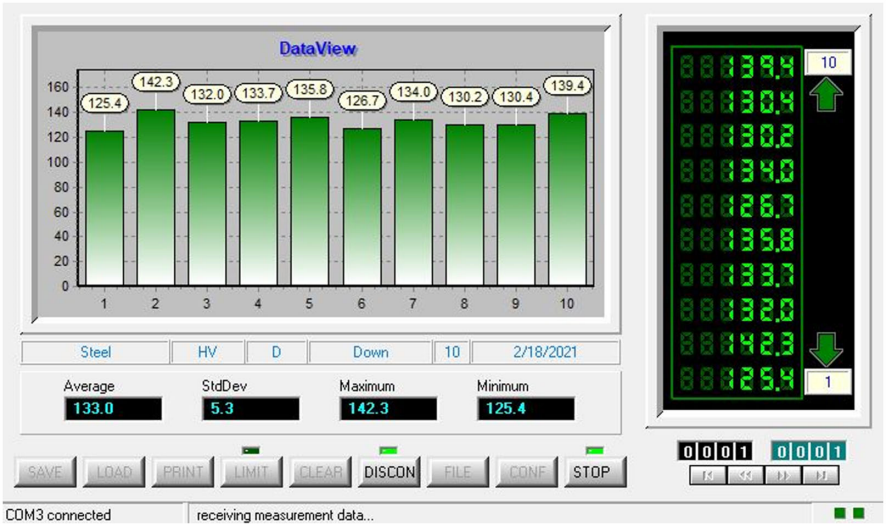

Figure 24
Distribution of hardness along the specimen at different die angles

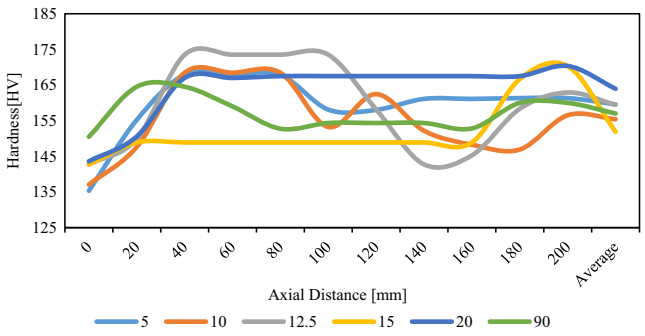

of the process with the target of modification of forged tube in the industrial forging process. In the future, research with an experimental part in the scope of microstructures can address the other concerns in this scope, although the current inquiry attempted to take into account every parameter of the forging process. The obtained results include the distribution of residual stress, velocity, the coordinate of the neutral plate, temperature, density, and distribution of hardness. The validation of the finite element model has been carried out through the hardness test on the forged tube by portable hardness tester.

Therefore, the results can be summarized as follows:

1) Results based on shear friction are more accurate and valid than those based on coulomb friction. As friction increases, residual stress in the specimen will increase;
2) A die angle (α) of 10° produces the highest density in the specimen while above10°, other angles lead to lower densities;
3) As the die angle increases, the angle of the velocity layers (β) in the material increases. This can reduce the distance between the neutral plate and the end of the specimen, transferring it to the sizing area. As a result, the radial force increases;
4) Increasing the die angle increases residual stress in the die. Thus, for angles above 12.5°, residual stress in the die increases considerably, which indicates a decrease in the longevity of the die and an increase in die fatigue;
5) The highest hardness is obtained at an angle of 20°, which creates uniform hardness along the entire length of the specimen. The amount of hardness changes greatly at other angles.

Ethical Statement

This study does not contain any studies with human or animal subjects performed by any of the authors.

Conflicts of Interest

The authors declare that they have no conflicts of interest to this work.

Data Availability Statement

Data are available from the corresponding author upon reasonable request.

Author Contribution Statement

Saeed Darki: Conceptualization, Methodology, Software, Formal analysis, Investigation, Resources, Data curation, Writing – original draft, Writing – review & editing, Visualization, Project administration. **Evgeniy Yurevich Raskatov:** Software, Validation, Resources, Supervision.

References

[1] Afrasiab, H., Hamzekolaei, M. G., & Hassani, A. (2022). New insight into the radial forging process by an asymptotic-based axisymmetric analysis. *Applied Mathematical Modelling*, *102*, 811–827. https://doi.org/10.1016/j.apm.2021.10.030

[2] Du, Z., Xu, W., Wang, Z., Zhu, X., Wang, J., & Wang, H. (2024). Multi-objective optimization of concave radial forging process parameters based on response surface methodology and genetic algorithm. *The International Journal of Advanced Manufacturing Technology*, *130*, 5025–5044. https://doi.org/10.1007/s00170-023-12888-8

[3] Ghaei, A., Karimi Taheri, A., & Movahhedy, M. R. (2006). A new upper bound solution for analysis of the radial forging process. *International Journal of Mechanical Sciences*, *48*(11), 1264–1272. https://doi.org/10.1016/j.ijmecsci.2006.06.002

[4] Groche, P., & Krech, M. (2017). Efficient production of sensory machine elements by a two-stage rotary swaging process—Relevant phenomena and numerical modelling. *Journal of Materials Processing Technology*, *242*, 205–217. https://doi.org/10.1016/j.jmatprotec.2016.11.034

[5] Herrmann, M., Schenck, C., & Kuhfuss, B. (2016). Dry rotary swaging with structured tools. *Procedia CIRP*, *40*, 653–658. https://doi.org/10.1016/j.procir.2016.01.150

[6] Jiang, H., Wang, Y., Dong, P., Zhang, P., Zhang, C., Zhu, C., . . . , & Zhao, S. (2024). Microstructure characteristics of the 2A50 aluminum alloy in radial forging and isothermal treatment conditions. *Journal of Materials Research and Technology*, *30*, 5258–5265. https://doi.org/10.1016/j.jmrt.2024.04.215

[7] Kumar, A., Kulkarni, R. R., & Ohdar, R. (2023). Towards understanding the behavior of magnesium alloy during different forging processes: An overview. *Materials Today: Proceedings*. Advance online publication. https://doi.org/10.1016/j.matpr.2023.03.448

[8] Li, H.-X., Wang, K., Luo, R., Zhu, Z.-Z., Deng, S., Luo, R., . . . , & Fang, F.-S. (2020). Influence of radial forging process on strain inhomogeneity of hollow gear shaft using finite element method and orthogonal design. *Journal of Central South University*, *27*, 1666–1677. https://doi.org/10.1007/s11771-020-4398-7

[9] Liu, Y., Herrmann, M., Schenck, C., & Kuhfuss, B. (2019). Plastic deformation components in mandrel free infeed rotary swaging of tubes. *Procedia Manufacturing*, *27*, 33–38. https://doi.org/10.1016/j.promfg.2018.12.040

[10] Li, K., Zhao, S., Zhang, D., & Zhang, C. (2024). Study on effect of single-tooth radial forging process parameters on spline shaft forming. In Z. Liu, R. Li, X. He, & Z. Zhu (Eds.), *Advances and challenges in advanced unmanned aerial systems* (pp. 485–493). Springer. https://doi.org/10.1007/978-981-99-8045-1_41

[11] Mahdavi, M. M., & Haghighat, H. A. (2019). On the optimum die angle in rod drawing process considering strain-hardening effect of material. *Iranian Journal of Mechanical Engineering Transactions of the ISME*, *20*(1), 113–128.

[12] Moumi, E., Ishkina, S., Kuhfuss, B., Hochrainer, T., Struss, A., & Hunkel, M. (2014). 2D-simulation of material flow during infeed rotary swaging using finite element method. *Procedia Engineering*, *81*, 2342–2347. https://doi.org/10.1016/j.proeng.2014.10.331

[13] Sanjari, M., Saidi, P., Karimi Taheri, A., & Hossein-Zadeh, M. (2012). Determination of strain field and heterogeneity in radial forging of tube using finite element method and microhardness test. *Materials & Design*, *38*, 147–153. https://doi.org/10.1016/j.matdes.2012.01.048

[14] Wang, Y., Xiong, L., Feng, D., Zhao, S., & Guo, Y. (2024). Investigation of the penetration performance of the radial forging process for wrought aluminium alloy. *Materials*, *17*(9), 2065. https://doi.org/10.3390/ma17092065

[15] Wu, Y., & Dong, X. (2016). An upper bound model with continuous velocity field for strain inhomogeneity analysis in radial forging process. *International Journal of Mechanical Sciences*, *115–116*, 385–391. https://doi.org/10.1016/j.ijmecsci.2016.07.025

[16] Wu, Y., Dong, X., & Yu, Q. (2015). Upper bound analysis of axial metal flow inhomogeneity in radial forging process. *International Journal of Mechanical Sciences*, *93*, 102–110. https://doi.org/10.1016/j.ijmecsci.2015.01.012

[17] Yang, Y., Yang, C., & Xu, C. (2024). Inhomogeneous deformation in the radial direction of the cold radial forged 30SiMn2MoVA steel tube. *Materials Chemistry and Physics*, 327. https://doi.org/10.1016/j.matchemphys.2024.129899

[18] Yang, Y., Fan, L., & Xu, C. (2022). Formation criterion of fissure defects in the inner wall of the radial forged steel tube. *The International Journal of Advanced Manufacturing Technology*, *123*, 3647–3655. https://doi.org/10.1007/s00170-022-10453-3

[19] Yang, Y., Fan, L., & Xu, C. (2020). The microstructure, texture evolution and plasticity anisotropy of 30SiMn2MoVA high strength alloy steel tube processed by cold radial forging. *Materials Characterization*, *169*, 110641. https://doi.org/10.1016/j.matchar.2020.110641

[20] Zou, J., Ma, L., Zhu, Y., Jia, W., Han, T., Yuan, Y., & Qin, G. (2021). Deformation mechanism of ZK60 magnesium bars during radial forging: Mathematical modeling and experimental investigation. *Materials Characterization*, *179*, 111321. https://doi.org/10.1016/j.matchar.2021.111321

[21] Zou, J., Ma, L., Zhu, Y., Qin, L., & Yuan, Y. (2024). Gradient microstructure and superior strength–ductility synergy of AZ61 magnesium alloy bars processed by radial forging with different deformation temperatures. *Journal of Materials Science & Technology*, *170*, 65–77. https://doi.org/10.1016/j.jmst.2023.07.003

[22] Zuev, L. B., Shlyakhova, G. V., & Barannikova, S. A. (2020). Effect of radial forging on the microstructure and mechanical properties of Ti-based alloys. *Metals*, *10*(11), 1488. https://doi.org/10.3390/met10111488

[23] Darki, S., & Raskatov, E. Y. (2020). Analysis of the hot radial forging process according to the finite element method. *The International Journal of Advanced Manufacturing Technology*, *110*, 1061–1070. https://doi.org/10.1007/s00170-020-05852-3

[24] Darki, S., & Raskatov, E. Y. (2023). Development of an analysis method for radial forging parameters based on hardness criterion. *Journal of Mechanical Engineering*, *20*(1), 149–167. https://doi.org/10.24191/jmeche.v20i1.21084

How to Cite: Darki, S., & Raskatov, E. Y. (2026). Investigations of the Hybrid Effects of the Operational Parameters in the Radial Forging Process Based on the Validation of the Hardness Test. *Archives of Advanced Engineering Science*, *4*(1), 51–64. https://doi.org/10.47852/bonviewAAES52024621